Multivariate prediction of functional outcome using lesion topography characterized by acute diffusion tensor imaging

Eric Moulton, Romain Valabrègue, Stéphane Lehéricy, Yves Samson, Charlotte Rosso

NeuroImage: Clinical 23 (2019) 101821

Contents lists available at ScienceDirect

NeuroImage: Clinical

journal homepage: www.elsevier.com/locate/ynicl

Multivariate prediction of functional outcome using lesion topography characterized by acute diffusion tensor imaging

Eric Moulton[a], Romain Valabregue[a,b], Stéphane Lehéricy[a,b,c,d], Yves Samson[a,e], Charlotte Rosso[a,c,e,*]

[a] Institut du Cerveau et de la Moelle épinière, ICM, Inserm U 1127, CNRS UMR 7225, Sorbonne Université, F-75013 Paris, France
[b] Centre de Neuro-Imagerie de Recherche, CENIR, ICM, Paris, France
[c] ICM Team Movement Investigation and Therapeutics, France
[d] AP-HP, Department of Neuroradiology, Hôpital Pitié-Salpêtrière, Paris, France
[e] AP-HP, Urgences Cérébro-Vasculaires, Hôpital Pitié-Salpêtrière, Paris, France

ARTICLE INFO

Keywords:
Acute stroke
Prediction
Prognosis
Functional outcome
Diffusion tensor imaging

ABSTRACT

The relationship between stroke topography and functional outcome has largely been studied with binary manual lesion segmentations. However, stroke topography may be better characterized by continuous variables capable of reflecting the severity of ischemia, which may be more pertinent for long-term outcome. Diffusion Tensor Imaging (DTI) constitutes a powerful means of quantifying the degree of acute ischemia and its potential relation to functional outcome. Our aim was to investigate whether using more clinically pertinent imaging parameters with powerful machine learning techniques could improve prediction models and thus provide valuable insight on critical brain areas important for long-term outcome. Eighty-seven thrombolyzed patients underwent a DTI sequence at 24 h post-stroke. Functional outcome was evaluated at 3 months post-stroke with the modified Rankin Score and was dichotomized into good (mRS ≤ 2) and poor (mRS > 2) outcome. We used support vector machines (SVM) to classify patients into good vs. poor outcome and evaluate the accuracy of different models built with fractional anisotropy, mean diffusivity, axial diffusivity, radial diffusivity asymmetry maps, and lesion segmentations in combination with lesion volume, age, recanalization status, and thrombectomy treatment. SVM classifiers built with axial diffusivity maps yielded the best accuracy of all imaging parameters (median [IQR] accuracy = 82.8 [79.3–86.2]%), compared to that of lesion segmentations (76.7 [73.3–82.8]%) when predicting 3-month functional outcome. The analysis revealed a strong contribution of clinical variables, notably – in descending order – lesion volume, thrombectomy treatment, and recanalization status, in addition to the deep white matter at the crossroads of major white matter tracts, represented by brain regions where model weights were highest. Axial diffusivity is a more appropriate imaging marker to characterize stroke topography for predicting long-term outcome than binary lesion segmentations.

1. Introduction

While clinical variables such as initial stroke severity, age, and lesion volume are useful in determining long-term outcome assessed by the modified Rankin Score (mRS), recent work has shed light on the independent predictive power of early ischemic stroke topography (Cheng et al., 2014; Duncan et al., 2000; Rosso et al., 2011; Wu et al., 2015; Yoo et al., 2010). In particular, damage to deep white matter at the crossroads of major white matter pathways has been shown to play a critical role in the level of autonomy patients can expect after an ischemic stroke (Rosso et al., 2011). In the majority of these studies, lesion topography is often represented as binary segmentations of abnormal regions on clinical diffusion weighted imaging (DWI) or FLAIR sequences. However, at the acute stage, the mere presence or absence of a lesion (binary segmentation) might be less informative than continuous variables capable of reflecting the severity of ischemia, which could be more pertinent for long-term outcome. The diffusion tensor imaging (DTI) model can reliably quantify tissue microstructure and thus constitutes a powerful means of evaluating the degree of ischemia at the acute stage of stroke (Beaulieu, 2002; Sotak, 2002). While, fractional anisotropy (FA) has proven a noteworthy biomarker at the subacute-chronic stage, there is now substantial evidence that axial diffusivity (AD) instead of FA is able to accurately reflect acute axonal damage related to subacute and chronic motor and global outcome

* Corresponding author at: Urgences Cérébro-Vasculaires, 47-83 Boulevard de l'Hôpital, 75013 Paris, France.
E-mail address: charlotte.rosso@aphp.fr (C. Rosso).

https://doi.org/10.1016/j.nicl.2019.101821
Received 14 December 2018; Received in revised form 3 April 2019; Accepted 8 April 2019
Available online 10 April 2019

(Doughty et al., 2016; Groisser et al., 2014; Liu et al., 2018; Moulton et al., 2015; Spampinato et al., 2017). Whether the severity of ischemia assessed with continuous DTI parameter maps and the presence or absence of an infarct using binary lesion segmentations harbor different prognostic values, however, remains to be elucidated.

Studying the effect of stroke topography on functional outcome using machine learning techniques has become increasingly popular due to their ability to account for complex interactions between brain regions (Price et al., 2017). Unlike commonly used mass-univariate analyses such as Voxel-based Lesion Symptom Mapping (VLSM) (Bates et al., 2003), multivariate methods can represent the relation of damage at every voxel to all other voxels. These methods are therefore highly adapted for predicting multifaceted clinical outcome scores, such as the mRS, which can reflect deficits covering several functional domains, namely motor, language, and spatial attention (Cheng et al., 2014). The relationship between functional outcome, evaluated by the mRS, and stroke topography has already been studied with both univariate and multivariate analyses using lesion segmentations (Cheng et al., 2014; Ernst et al., 2018; Munsch et al., 2016; Wu et al., 2015) and also with apparent diffusion coefficient (ADC) maps (Cuingnet et al., 2011; Rosso et al., 2011) acquired at the acute stage; however, to our knowledge, no whole-brain study has been performed with acute DTI images. In this study, we take advantage of a large dataset of thrombolyzed stroke patients who underwent a DTI imaging protocol at 24 h post-stroke and a sophisticated machine learning pipeline to evaluate the prognostic value of DTI-derived parameters and lesion segmentations.

Our goals were to (1) evaluate the predictive power of the DTI-derived parameter maps generated at the acute stage as well as lesion segmentations in classifying good vs. poor outcome using support vector machine (SVM) classifiers, (2) determine if certain DTI maps yield better classification rates than lesion segmentations, and (3) infer which brain regions contribute the most to functional outcome by investigating the weights of the best performing model. We predicted that classification accuracy would differ among the four classical DTI parameters, considering the varying degrees to which each one reflects acute stroke damage. Furthermore, we hypothesized that the severity (i.e., continuous changes in diffusivity) rather than the presence or absence of ischemia (i.e., binary lesion segmentation) would be able to better capture brain damage affecting long-term functional outcome. Finally, in concordance with previous findings, we expected damage to deep white matter to play an influential role in distinguishing good vs. poor outcome, due to the simultaneous multiple disconnections that may arise at the intersection of long-range pathways.

2. Materials and methods

2.1. Patients

Two hundred ninety-seven patients were retrospectively screened from September 1, 2013 until April 30th, 2018 at the Urgences Cérébrovasculaires at the Hôpital de la Pitié Salpêtrière. Inclusion criteria for this cohort were: (1) MRI-demonstrated ischemic stroke of the carotid territory, (2) thrombolysis treatment within 4.5 h after stroke onset, (3) follow-up MRI access at 24 h post-stroke, (4) interpretable recanalization status, and (5) clinical assessment using the modified Rank Score (mRS) at 3 months post-stroke. Thrombolytic treatment was administered according to the American Stroke Stroke Association and the European Stroke Organization guidelines (0.9 mg/kg, maximal dose 90 mg) (Jauch et al., 2013). Patients with bilateral lesions were deemed suitable for analysis if clinical symptoms were lateralized to one hemisphere (e.g., unilateral hemiparesis, aphasia without neglect, etc.). For these patients, the affected hemisphere was considered as that which caused clinical symptoms. Exclusion criteria were (1) overly artifacted imaging data, (2) dependence on external aid before the stroke or the reoccurrence of stroke before the 3-month follow-up, (3) death before the 3-month follow-up.

A mRS score was recorded at the 3-month follow-up through a physical examination with a neurologist at our hospital or through a structured telephone interview. The primary outcome measure of this study was a dichotomized mRS score for good ($mRS \leq 2$) and poor ($mRS > 2$) outcome. Descriptive statistics consisted of median and interquartile ranges (IQR). All imaging and clinical data were obtained during routine clinical workup in our stroke center. According to French legislation, explicit informed consent was therefore waived. The study was approved by the Pitié-Salpêtrière Hospital Ethics Committee.

2.2. Image acquisition

Imaging data used in this study are from our emergency stroke unit in which we examined patients with typical DWI sequences but also a DTI protocol. Twenty-four hours after admission, patients underwent a follow-up MRI with a 3 T MR750 MRI scanner (General Electric) with an 8-channel coil. The following DWI sequences were used for the current analysis: (1) an averaged 3-direction DWI ($b = 1000\,s/mm^2$, TR = 11,700 ms, TE = 72.3 ms, matrix size = 256 × 256, slice number = 48, voxel size = $0.94 \times 0.94 \times 3\,mm^3$, acquisition time = 0:59 min) and (2) a 30-direction DWI (2 $b = 0\,s/mm^2$ images followed by 30 non-collinear diffusion-encoding gradients at $b = 1000\,s/mm^2$, TR = 12,000 ms, TE = 82.3 ms, matrix size = 256 × 256, slice number = 44, voxel size = $1.09 \times 1.09 \times 3\,mm^3$, acquisition time = 6:36 min).

2.3. Image processing

Image processing served to prepare data for classification in a common reference space and was performed using a pipeline optimal for diffusion MRI data at the acute stroke stage as previously described (Moulton et al., 2018). In brief, after correcting for (1) denoising (Veraart et al., 2016a, 2016b), (2) eddy currents and head motion using FSL's EDDY with slice interpolation for slices with significant signal drop (Andersson et al., 2016; Andersson and Sotiropoulos, 2016), and (3) bias-field correction (Zhang et al., 2001), FA, AD, mean diffusivity (MD), and radial diffusivity (RD) maps were calculated from a tensor model estimated using FSL's DTIFIT (Basser et al., 1994; Smith et al., 2004), and brains were skull stripped (Smith, 2002). Lesion segmentation was performed by identifying hypersignal regions on the 3-direction DWI sequence image and co-registered to the DTI maps. To process all images in the same hemisphere, both native and flipped DTI maps as well as lesion segmentations were registered to an in-house healthy-subject FA template using Advanced Normalization Tools (ANTs) with lesion masking (Supplementary Materials). Since flipping was performed before normalization, both hemispheres were registered to the same anatomical landmarks in our FA template. This reduced the impact of any natural structural asymmetries – such as Petalia and Yakovlevian torque or within Perisylvian gyri and sulci (Toga and Thompson, 2003) – on the calculation of the laterality indices between homologous regions of both hemispheres.

In stroke imaging, it is common practice to analyze relative differences between the affected and unaffected hemispheres rather than absolute values of the affected hemisphere alone. To this end, we kept all affected hemispheres to the same side and constructed laterality index (LI) maps, hereafter referred to as asymmetry maps, using the normalized native and flipped DTI maps with the following equation at each voxel: (affected-unaffected)/(affected + unaffected). The LI is a score between −1 and 1 for which the negative range indicates smaller values on the affected side and the positive range indicates larger values on the affected side. Acute stroke is largely characterized by strong decreases in diffusivity with respect to the unaffected hemisphere, which can be seen as negative values on the MD, AD, or RD asymmetry maps (Fig. 1). We also applied a modest 2 mm Gaussian smoothing to the asymmetry maps to compensate for imperfections in normalization while conserving the specificity of each region (Samper-González et al., 2018). Since asymmetry maps are highly symmetrical, our analysis can

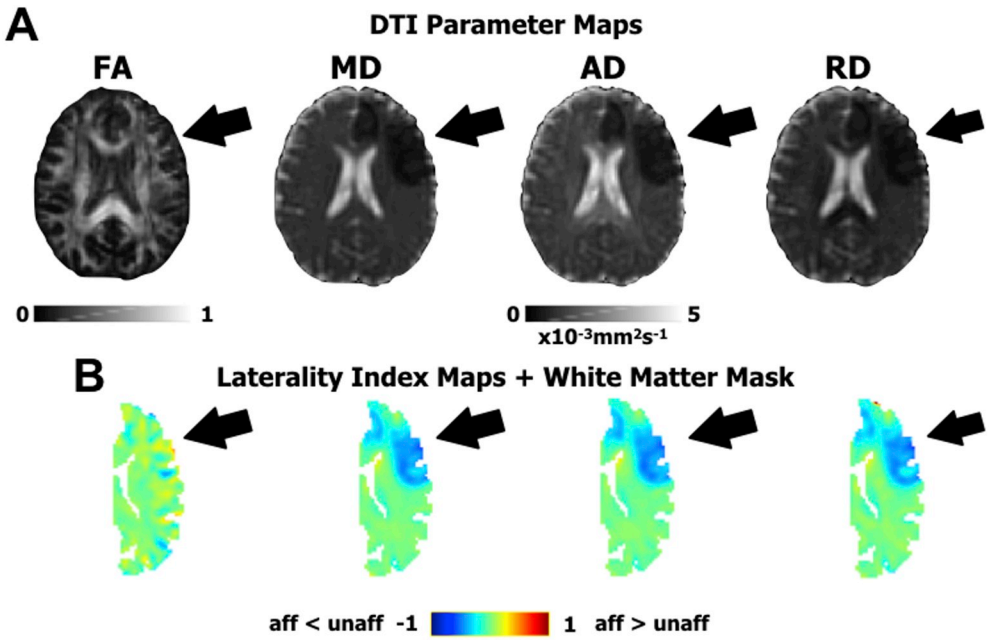

Fig. 1. Diffusion Tensor Imaging (DTI) features. A. The four DTI parameter maps for a representative acute stroke patient. From left to right: Fractional Anisotropy (FA), Mean Diffusivity (MD), Axial Diffusivity (AD), and Radial Diffusivity (RD). B. The corresponding Laterality Index (LI) or asymmetry maps in a white matter mask used to create prediction models. The black arrow indicates the presence of acute ischemia, shown as an area of low diffusivity on MD, AD, and RD maps and negative regions on the respective LI maps. Acute ischemia is poorly seen on the FA map.

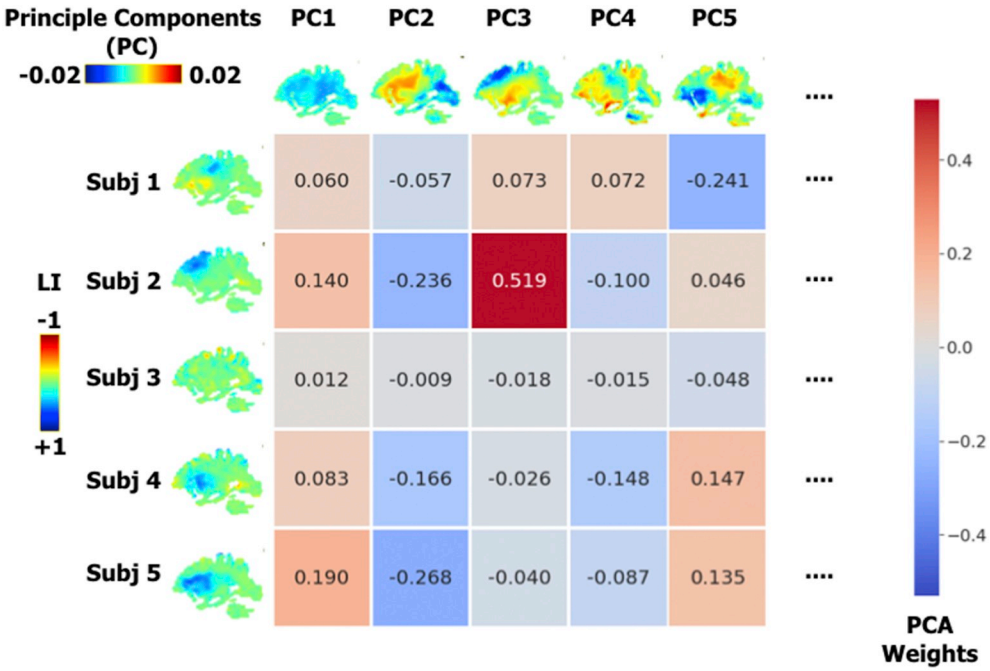

Fig. 2. Dimensionality reduction with Principle Component Analysis (PCA). PCA allows for the reconstruction of each subject's (subj) imaging data through a linear combination of principle components (PC), which reflect representative patterns over the studied population. The coefficients of each PC used to reconstruct each subject's imaging data become the features for the classifier. For illustrative purposes, shown here is the PCA analysis for AD asymmetry maps (LI) over the whole cohort, whereas independent PCAs are performed for each cross-validation split.

be reliably restrained to one hemisphere. Moreover, relative differences in diffusivity are more pronounced in white matter than grey matter regions (Bhagat et al., 2008; Muñoz Maniega et al., 2004; Yang et al., 1999). With these considerations, we restricted our analysis to a hemispheric white matter mask by thresholding the FA template at 0.2 and manually filling in potential holes in the mask, such as those in the basal ganglia. The white matter mask also aided in removing imperfections in normalization at the cortical level.

2.4. Model estimation and validation

We sought to classify patients into good vs. poor outcome at 3 months post-stroke with imaging data at 24 h post-stroke and baseline clinical variables using a support vector machine (SVM) as implemented in scikit-learn in Python (Abraham et al., 2014). SVMs are useful machine learning techniques used in neuroimaging (see Lemm et al. (2011) for a detailed explanation of SVMs and Rondina et al. (2017) for an illustrative application to stroke imaging), have already proven effective in explaining various categories of stroke-related deficits, and are compatible with structural imaging data (Cuingnet et al., 2011; Mah et al., 2014; Mateos-Pérez et al., 2018; Rondina et al., 2016; Yourganov et al., 2015; Zhang et al., 2014). Here, we estimated and validated classification models using different imaging modalities (i.e., DTI-derived asymmetry maps or lesion segmentations) along with important clinical variables considered to be independent predictors of stroke outcome, notably recanalization status, thrombectomy treatment, age, and lesion volume. Recanalization status (complete or not) and thrombectomy treatment (received or not) were treated as binary variables. As in similar studies (Wu et al., 2015), we did not include baseline NIHSS as a feature since it already reflects the extent of brain

damage and can be predicted from stroke topography (Phan et al., 2010). Including this variable prevents us from addressing our specific goals of disentangling the predictive value of each imaging parameter and thus investigating the best model's spatial weights. However, for the interest of the reader, we also evaluated the same SVM models including Day 1 NIHSS scores (N = 85) in addition to a non-imaging model with only clinical variables.

In machine learning and neuroimaging, there is often a disproportionate ratio of features (here, voxels) for available observations (i.e., patients). This imbalance is commonly referred to as the curse of dimensionality and can hinder the predictive power of multivariate models. Therefore, we introduced a principle component analysis (PCA) step for imaging data in our model construction pipeline in order to reduce the dimensionality of our data (Fig. 2). In fact, PCA presents a double advantage in machine learning analyses with stroke patients. The most obvious advantage is that the number of features will be, at most, one less than the number of observations (when there are more features than observations). The second advantage of PCA stems from the fact that, in stroke, lesioned voxels do not arise randomly but co-occur according to the vascular tree (Mah et al., 2014). At the population level, therefore, recurrent patterns of diffusivity asymmetries and stroke lesions will be present across patients and can form a new basis for explaining them. In other words, we can describe diffusivity asymmetries or lesioned voxels by a weighted sum of representative patterns of these parameters instead of tens of thousands of voxels (38,807 in our case). These weights in PCA-space then become the features for our classifier. We did not choose the number of principle components *a priori*, contrary to other studies that have used explained variance criteria (Corbetta et al., 2015; Siegel et al., 2016). Rather, we decided to introduce the number of principle components to retain as a hyper-parameter to be optimized (i.e., maximize classification accuracy) as explained below.

We employed repeated stratified nested cross-validation (CV) for the unbiased construction and evaluation of our classifiers, according to the recommendations in Varoquaux et al. (2017) (Supplementary Fig. 1). In our nested CV, an inner 2-fold CV loop first builds models with optimized hyperparameters (i.e., the set of the number of principle components and the L2-regularization constant that maximizes classification accuracy), and an outer 3-fold CV loop then yields unbiased evaluations of the constructed model. With this CV scheme, we ensured not only an equal partition of our data set in all loops but also an equal proportion of good:poor class observations. Furthermore, models were constructed with a misclassification penalty weighted by class balance. To bypass the computational time required to determine the optimal set of hyperparameters, for each inner CV loop, we randomly chose 60 candidate values from a discrete uniform distribution for possible principle components (1–87) and a reciprocal distribution for regularization constants (1×10^{-3} to 1×10^{6}). Random searches over parameter space have been found to be as good as or better than systematic grid searches with significant gains in computational time (Bergstra and Bengio, 2012). In our case, using 60 candidate values ensured that we had a 95% chance of being within a 5% interval of the best parameter set. This procedure was repeated 500 times in order to obtain a reliable point-estimate of model accuracy with an associated confidence interval. For each imaging modality, we herein summarize classification accuracy, sensitivity, and specificity as the median with the interquartile range (IQR) over CV splits. We chose to not compare these performance metrics with statistical tests as the statistical comparison of machine learning models across cross-validation loops is a complex matter for which there is no universal solution. Many studies have employed standard paired *t*-tests across cross-validation results; however, this method yields extremely liberal p-values and is strongly advised against (Nadeau and Bengio, 2003). Adaptations have been proposed, yet these methods are dependent on the cross-validation scheme and, in particular, favor datasets in which many outer CV loops can be afforded (Nadeau and Bengio, 2003). In our study, we chose to use few but large CV splits – instead of many but small CV splits (such as leave-one-out CV) – in order to properly estimate our models with our relatively small dataset as recommended by Varoquaux (2018). Our CV scheme was therefore not compatible with the adaptations to classical statistical comparisons. However, in order to demonstrate that individual model accuracy significantly differed from chance, we ran permutation tests with 1000 iterations to reconstruct the sampling distribution of the underlying null hypothesis.

To gain insight on the underlying anatomical determinants of long-term outcome, we inspected the model of the imaging modality that yielded the highest median classification accuracy. For this model, we projected the SVM model weights back onto the brain from PCA-space and calculated the average over all CV folds (Rondina et al., 2017; Varoquaux et al., 2017). The resulting map reflected the relative importance of each brain region in classifying groups. We created a region of interest (ROI) composed of the largest connected component of voxels with the strongest weights (95th percentile) associated with larger decreases in diffusivity or higher lesion incidence in patients with poor outcome, depending on the winning model. We then used this ROI to investigate the involvement of well-known long-range white matter tracts in functional outcome in a tractography analysis using a whole-brain connectome performed on the in-house template (Moulton et al., 2018) (Supplementary Materials).

3. Results

3.1. Patient cohort

Out of the prospective 297 patients, 87 were retained for the final analysis (Fig. 3, Table 1). Maximum lesion overlap was in the putamen, external capsule, and caudate nucleus (35–40%, N = 31–36), reflecting typical lesions of the middle cerebral artery territory of a clinical population (Phan et al., 2005) (Supplementary Fig. 2). Two patients had bilateral lesions, with a main lesion presumed to be the cause of neurological deficits, and infracentimetric lesions on the contralateral side (Supplementary Fig. 2).

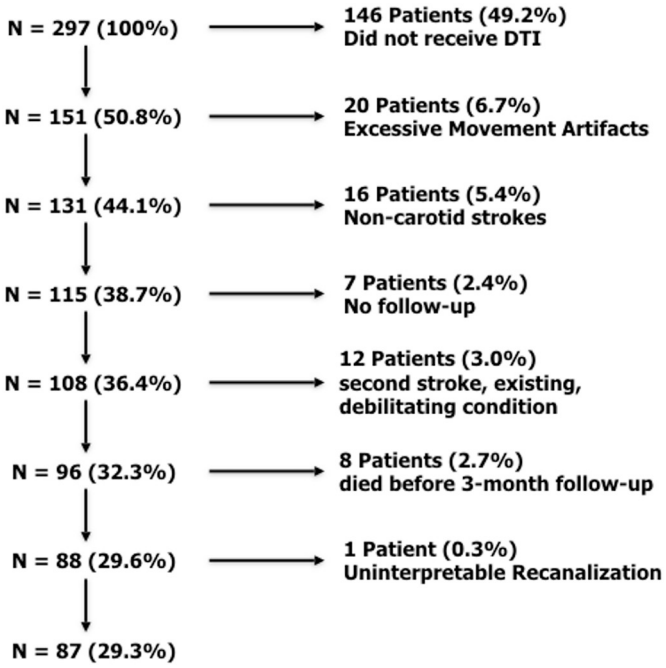

Fig. 3. Patient inclusion flowchart.

Table 1
Patient cohort descriptive statistics.

Age (years)	71.1 [57.1–80.8]
Female N (%)	39 (44.8%)
NIHSS Admission (N = 87)	11.5 [7.3–20.0]
NIHSS Day 1 (N = 85)	4.5 [2.0–12.0]
NIHSS Day 7 (N = 62)	2.0 [0.0–9.5]
Time to MRI (min) (N = 87)	110.0 [78.0–170.0]
Time to rtPA (min) (N = 87)	140.0 [110.8–202.3]
DWI Lesion Volume (mL) (N = 87)	12.4 [4.2–45.1]
Received Thrombectomy N (%)	32 (36.8%)
Complete Recanalization N (%)	62 (71.3%)
Pure MCA stroke N (%)	81 (92.0%)
Mixed MCA-ACA stroke N (%)	2 (2.3%)
Mixed MCA-PCA stroke N (%)	4 (4.6%)
Mixed MCA-ICA stroke N (%)	1 (1.1%)
Left Lesions N (%)	58 (66.6%)
Good Outcome (mRS ≤ 2) N (%)	61 (70.1%)

3.2. Model evaluation

Model performance differed for each imaging modality (Table 2). In particular, AD asymmetry maps yielded the highest median accuracy (82.8%), sensitivity (80.0%), and specificity (84.0%). MD asymmetry maps performed slightly less well, closely followed by RD. Finally, classifiers with lesion segmentation and FA performed the worst, both yielding median accuracies of 76.7%. In other words, a model based on AD maps would result in a false prediction for one out of every six patients in a clinical setting, whereas, a model based on FA maps or lesion segmentation would result in a false prediction for one out of every four patients. All model accuracies were statistically significant ($p < .003$).

Each type of model found different numbers of principle components optimal for classification (Table 2). Models built with AD, MD, RD asymmetry maps and lesion segmentations retained principle components explaining the variance of much of the data (77.5%–89.0%). On the other hand, classifiers with FA asymmetry maps retained only 53.2% of the variance in the data.

In order to verify that the results did not depend on an unequal distribution of good vs. poor outcome, despite the misclassification penalty used to construct our models, we performed two alternate analyses. In the first, we incorporated a random under-sampling of the overrepresented class (i.e., good outcome) in the inner cross-validation loop; in the second, we incorporated an up-sampling technique of the underrepresented class (i.e., poor outcome) by generating new data points by interpolation (Chawla et al., 2002). Accuracy results remained rather similar (Supplementary Tables 1,2).

Of note, the non-imaging model with Day 1 NIHSS (plus the other clinical predictors) reached a prediction accuracy of 89.3%, and the inclusion of AD asymmetry maps yielded a model reaching the same accuracy. The accuracy was slightly less with the inclusion of other imaging maps yet was higher than the models without Day 1 NIHSS, suggesting that the NIHSS drove classification independently of imaging data (Supplementary Table 3). Indeed, considerably fewer principle components of the imaging data were required to maximize classification accuracy in these models (Supplementary Table 3), corroborating the notion that the NIHSS already encodes for lesion topography (Phan et al., 2010). Therefore, in order to answer the objectives of the current study, the remainder of the manuscript will refer to the SVM models without the NIHSS.

For the winning model constructed with AD asymmetry maps, the clinical variable with the strongest influence on outcome was lesion volume (indicating that smaller lesion volumes were associated with good prognosis), followed by thrombectomy treatment (receiving thrombectomy treatment resulted in good outcome) and less so by recanalization status (patients with complete recanalization had good outcome) (Fig. 4). As for imaging data, the strongest SVM weights formed a large cluster in the deep MCA territory (Fig. 4). The tractography analysis revealed that this region largely corresponded to the deep white matter at the crossroads of corticofugal and long-range association pathways, such as the corticospinal tract, the corpus callosum, the long, anterior, and posterior segments of the arcuate fasciculus, the second and third branches of the superior longitudinal fasciculus, and the frontal aslant tract (Fig. 5).

4. Discussion

We used early DTI in combination with baseline clinical data in a large cohort of acute stroke patients to power a sophisticated machine learning pipeline aimed at classifying good vs. poor functional outcome. We found that AD was able to best classify long-term outcome, much better than FA or commonly used lesion segmentations. As expected, we found a strong contribution from clinical variables, notably – in decreasing order – lesion volume, thrombectomy treatment, and recanalization status. In addition, we found that the most influential brain areas on outcome were highly concordant with previous studies, supporting the validity of our results.

The novelty of our study lies within the systematic availability of DTI data at 24 h post-stroke to investigate the effect of stroke topography on long-term outcome. This unique data set differs from similar studies performed at the acute phase which have primarily resorted to clinical DWI or FLAIR sequences for lesion segmentation to address this question (Cheng et al., 2014; Ernst et al., 2018; Munsch et al., 2016; Wu et al., 2015). Moreover, while other studies have evaluated the predictive value of acute DTI biomarkers with correlation analyses (Groisser et al., 2014; Liu et al., 2018; Moulton et al., 2015; Spampinato et al., 2017), to our knowledge, this is the first study to use whole-brain DTI data in a multivariate framework for classifying functional outcome. Interestingly, in our study, we found that not only did AD asymmetry maps result in the highest classification accuracies of all DTI parameters, but they also outperformed commonly used binary lesion segmentations by 6.1%, resulting in an improvement of false prediction ratio of 1/4 to 1/6. This increase in accuracy was highly driven by a much larger sensitivity to predict poor outcome (66.7% for lesion segmentations vs. 80.0% for AD) rather than a marginally higher specificity to predict good outcome (81.8% for lesion segmentations vs.

Table 2
Model evaluation and construction. The median and interquartile range is shown over cross-validation splits for SVM models constructed with different imaging modalities. The number of principle components and explained variance thereof refer to automatically tuned hyper-parameters. Permutation test significant *$p < .003$.

Imaging Modality	Model Evaluation			Model Construction	
	Accuracy (%)	Sensitivity (%)	Specificity (%)	Number of Principle Components	Variance of Data Explained by PCs (%)
FA	76.7 [72.4–80.0]*	66.7 [57.1–80.0]	80.0 [76.2–83.3]	17 [9–24]	53.2 [38.2–64.1]
MD	80.0 [75.9–86.2]*	77.8 [66.7–88.9]	82.6 [79.2–86.4]	17 [9–25]	82.3 [70.3–87.8]
AD	82.8 [79.3–86.2]*	80.0 [66.7–88.9]	84.0 [80.0–88.2]	15 [8–24]	77.5 [66.0–85.0]
RD	79.3 [72.4–82.8]*	71.4 [60.0–83.3]	81.0 [77.3–85.7]	18 [9–26]	89.0 [81.2–93.4]
Lesion Segmentation	76.7 [73.3–82.8]*	66.7 [57.1–80.0]	81.8 [77.3–85.0]	15 [7–23]	80.7 [65.5–89.2]

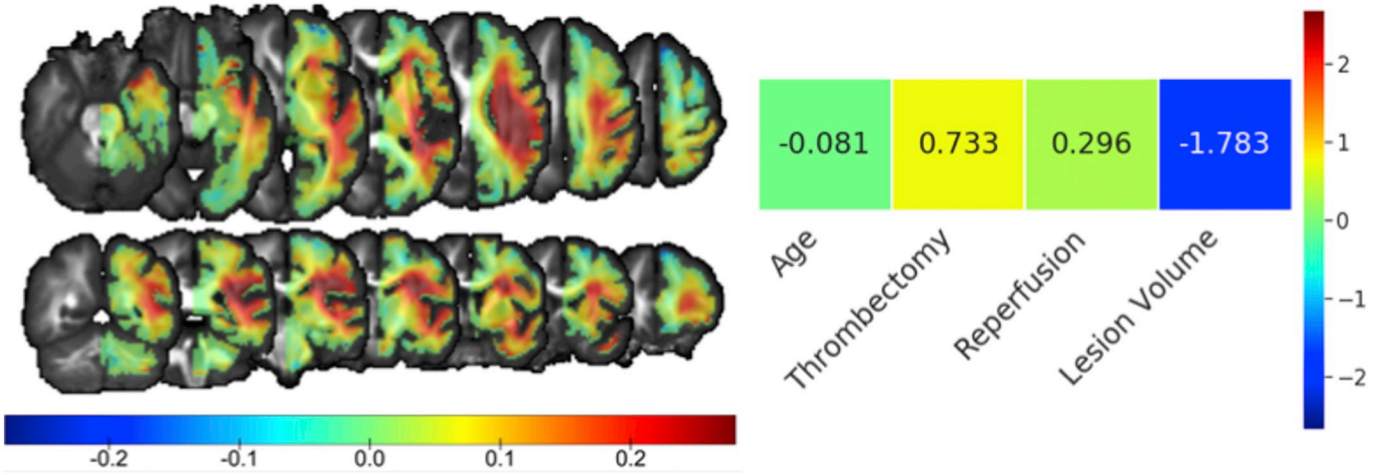

Fig. 4. Model weights of the SVM classifier using AD asymmetry maps and clinical variables. For imaging data, the weights represent the relative relevance of each brain region in classifying good vs. poor outcome on axial (top) and coronal (bottom) slices. Positive values indicate relatively lower AD asymmetries for patients with poor outcome compared with those with good outcome, and vice-versa. Separate color bars are used for the SVM weights of the imaging data and clinical variables due to the differences in scale.

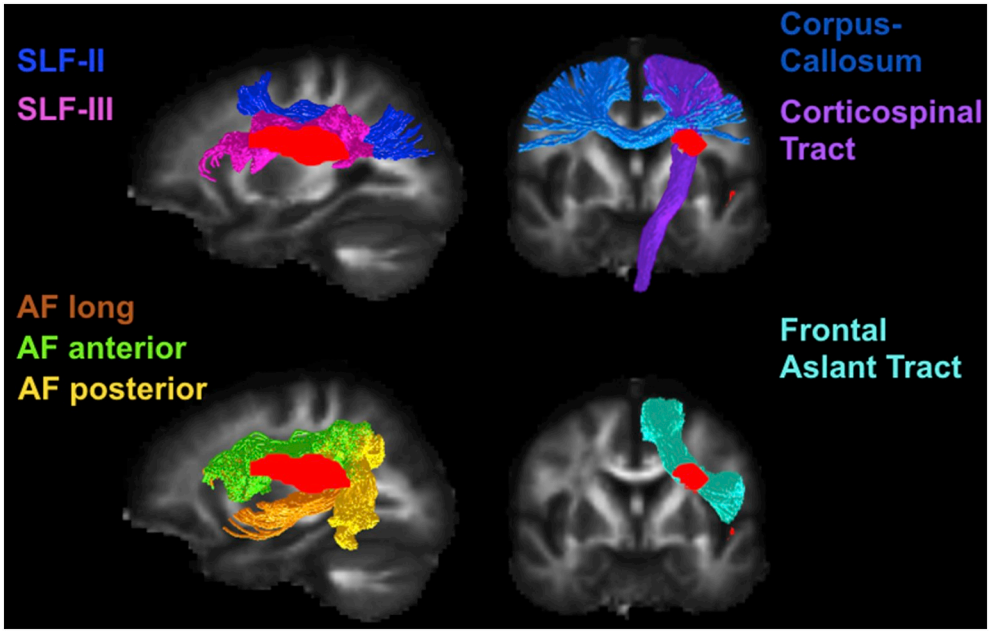

Fig. 5. Tractography analysis from the most influential regions for functional outcome. The most influential areas of lower axial diffusivity for patients with poor outcome (red cluster). Major corticofugal and long-range association tracts pass through this critical area, notably, the second and third branch of the superior longitudinal fasciculus (SLF), the corpus callosum, the corticospinal tract, the long, anterior, and posterior segments of the arcuate fasciculus (AF), and the frontal aslant tract.

84.0% for AD).

It is important to note that, considering the current study design, there was no *a priori* reason for all models to not achieve the same classification rate if not for the data driving them. Indeed, each model was given the same clinical scores along with the same partitions of imaging data over cross-validation loops and was free to optimize its own hyper-parameters to maximize accuracy. From this perspective, all imaging modalities were on an equal footing. The only limiting factor for each classifier, therefore, was the relevance – or lack thereof – of the imaging features used to train it. Indeed, in order to predict poor outcome, a proper imaging marker must be able to capture acute stroke damage (high sensitivity), whereas the ability to predict good outcome (high specificity) relies rather on the absence of diffusion abnormalities (i.e., asymmetry values of 0), a common feature between all imaging modalities. We can therefore conclude that there was truly something unique about the clinical pertinence of AD – compared to other candidate imaging parameters and beyond baseline clinical scores – in characterizing acute ischemia and its relationship to future outcome.

The superior classification performance of AD over other imaging modalities corroborates previous studies having reported higher correlations between acute AD abnormalities of the corticospinal tract and future motor and global outcome with respect to other DTI parameters (Groisser et al., 2014; Liu et al., 2018; Moulton et al., 2015; Spampinato et al., 2017). Acute changes in AD likely reflect increased intracellular viscosity from direct axonal damage as supported by recent DTI-immunohistology studies or neuronal beading (Baron et al., 2015; Budde and Frank, 2010; Sun et al., 2006). Moreover, from the acute to subacute stage, AD and RD follow different trajectories. While AD monotonically decreases over this time period partly from cell necrosis and axonal degeneration, RD first decreases, in part, due to cytotoxic oedema only to then increase following the deterioration of myelin sheaths (Liang et al., 2007). This switch in dynamics of RD happens within days post stroke onset, limiting its ability to characterize the degree of ischemia and thus its predictive power. The same limitations therefore apply to FA since it takes into account both AD and RD.

The most noteworthy result of our analysis is that continuous DTI variables, in particular AD, performed better than binary lesion segmentations, which have been the primary means for stroke topography

characterization. This result has important repercussions for the long-debated independent role of stroke topography vs. baseline clinical variables. For example, using voxel-based lesion symptom mapping (VLSM), two studies reported that, once corrected for lesion volume, lesion location was no longer related to the 3-month follow-up mRS in the right hemisphere but remained so in the left hemisphere (Ernst et al., 2018; Wu et al., 2015). Similarly, Munsch et al. (2016) used VLSM to identify eloquent brain regions associated with the 3-month mRS; in a separate analysis, they showed that the number of overlapping voxels between patients' lesions and the previously found eloquent cluster was not an independent predictor of good vs. poor outcome. While these studies have provided evidence that stroke location may not be as important as baseline clinical variables in predicting long-term outcome, our findings suggest that these previously reported negative results may arise from inadequately characterizing stroke topography with simple lesion segmentation. Furthermore, unlike models with binary lesion segmentations, which are constrained to areas of high infarct incidence, whole-brain diffusion maps can also take into account abnormalities at a distance from the lesion. In light of these considerations, right hemisphere and perhaps additional left hemisphere regions may still in fact highly contribute to long-term stroke outcome, if represented by more sensitive imaging markers.

Our SVM models with AD asymmetry maps revealed a spatially heterogeneous set of weights for classification. In particular, the weights corresponding to larger decreases in diffusivity for poor vs. good recovery formed a cluster in the white matter at the crossroads of many major fiber tracts governing motor, language, and attention, in concordance with many previous findings (Cheng et al., 2014; Cuingnet et al., 2011; Ernst et al., 2018; Munsch et al., 2016; Rosso et al., 2011; Wu et al., 2015). Importantly, this critical region was established through the contribution of different lesion topographies accounting for 77.5% of the variance in AD asymmetry maps, as identified with PCA. An interpretation of this result is that functional outcome is mostly governed by a subset of reoccurring lesion patterns, rather than individual voxels. In other words, it is the similarity between the spatial extent of a patient's lesion and these critical patterns that ultimately determines autonomy vs. dependence on external aid at 3 months post-stroke, supporting the significance of lesion topography (Corbetta et al., 2015). In fact, this procedure likely enabled us to overcome the fixed set of lesion patterns specific to our cohort and capture global lesion topographies that generalize to a typical population.

While we obtained high and clinically relevant accuracies with whole-brain acute DTI data, other imaging modalities such as functional MRI (fMRI) could have complemented this analysis in order to investigate whether it lead to a better classification of global outcome. Indeed, global outcome is a general reflection of deficits covering multiple domains, such as motor, language, and spatial neglect, which all depend on a mixture of not only structural but also functional brain abnormalities (Siegel et al., 2016). For instance, SVM with fMRI has already been shown to decode acute patterns of functional connectivity of the primary motor cortex for predicting motor deficits at both the acute (Rehme et al., 2015a) and chronic (Rehme et al., 2015b) phases of stroke. Similarly, task-based fMRI has been used at the acute stage of stroke with language paradigms to predict good vs. poor language outcome (Saur et al., 2010). Future studies should investigate the independent contributions of structural and functional imaging at the acute stage for long-term outcome.

A caveat of our study was our inability to disentangle the contribution of lesion side. Indeed, machine learning techniques require large datasets to build reliable models and evaluate their performance in an unbiased way (Varoquaux, 2018). For this reason, we were obliged to keep all lesions in the same hemisphere to maximize the amount of usable data. As mentioned, previous studies have highlighted differential effects of lesion topography for left vs. right lesions, either from a symptomatology (Cheng et al., 2014) or a clinical relevance (Ernst et al., 2018; Munsch et al., 2016; Wu et al., 2015) point-of-view. While our approach prevented us from further investigating this, our study provides a serious argument to revisit certain conclusions of these studies, since most of them have been performed with lesion segmentations. Moreover, our tractography analysis revealed a crucial role of fiber tracts involved in well-recognized lateralized functions, such as the arcuate fasciculus for language (Marchina et al., 2011; Rosso et al., 2015) and the SLF-II for neglect (Thiebaut de Schotten et al., 2014), suggesting that our model captured important structures of stroke topography for both left and right hemispheres.

A second limitation could be our restrained analysis to the white matter and inclusion of patients with stroke of the carotid territory. However, in a general clinical population, as in ours, infarcts of the carotid territory represent > 85% of all stroke and mostly occur in subcortical structures where DTI is most informative and important diffusion changes take place in response to acute ischemia (Bhagat et al., 2008; Muñoz Maniega et al., 2004; Phan et al., 2005; Yang et al., 1999).

5. Conclusion

In summary, this is the first study to investigate the effect of stroke topography on functional outcome evaluated with both DTI and lesion segmentations in a machine learning framework. Our study highlights the added benefit of axial diffusivity in addition to the limitations of binary lesion segmentation for quantifying acute ischemic stroke topography and its relation to long-term outcome. Our results have important implications for salvaging brain areas critical for functional outcome and can aid clinicians in weighing the costs, benefits, and risks for thrombolysis or thrombectomy treatments at the acute stroke stage.

Sources of funding

The Pitié-Salpêtrière registry was supported by the French Ministry of Health grant EVALUSINV PHRC AOM 03 008. The research leading to these results has received funding from “Investissements d'avenir” ANR-10-IAIHU-06 and ANR-11-INBS-0006.

Disclosures

None.

Declaration of interest

None.

Appendix A. Supplementary data

Supplementary data to this article can be found online at https://doi.org/10.1016/j.nicl.2019.101821.

References

Abraham, A., Pedregosa, F., Eickenberg, M., Gervais, P., Mueller, A., Kossaifi, J., Gramfort, A., Thirion, B., Varoquaux, G.G., Muller, A., Kossaifi, J., Gramfort, A., Thirion, B., Varoquaux, G.G., Mueller, A., Kossaifi, J., Gramfort, A., Thirion, B., Varoquaux, G.G., 2014. Machine learning for neuroimaging with scikit-learn. Front. Neuroinform. 8, 1–10. https://doi.org/10.3389/fninf.2014.00014.

Andersson, J.L.R., Sotiropoulos, S.N., 2016. An integrated approach to correction for off-resonance effects and subject movement in diffusion MR imaging. Neuroimage 125, 1063–1078. https://doi.org/10.1016/j.neuroimage.2015.10.019.

Andersson, J.L.R., Graham, M.S., Zsoldos, E., Sotiropoulos, S.N., 2016. Incorporating outlier detection and replacement into a non-parametric framework for movement and distortion correction of diffusion MR images. Neuroimage 141, 556–572. https://doi.org/10.1016/j.neuroimage.2016.06.058.

Baron, C.A.lla., Kate, M., Gioia, L., Butcher, K., Emery, D., Budde, M., Beaulieu, C., 2015. Reduction of diffusion-weighted imaging contrast of acute ischemic stroke at short diffusion times. Stroke. 46, 2136–2141. https://doi.org/10.1161/STROKEAHA.115.008815.

Basser, P.J., Mattiello, J., LeBihan, D., 1994. Estimation of the effective self-diffusion tensor from the NMR spin echo. J. Magn. Reson. B 103, 247–254.

Bates, E., Wilson, S.M., Saygin, A.P., Dick, F., Sereno, M.I., Knight, R.T., Dronkers, N.F., 2003. Voxel-based lesion–symptom mapping. Nat. Neurosci. 6, 448–450. https://doi.org/10.1038/nn1050.

Beaulieu, C., 2002. The basis of anisotropic water diffusion in the nervous system - a technical review. NMR Biomed. 15, 435–455. https://doi.org/10.1002/nbm.782.

Bergstra, J., Bengio, Y., 2012. Random search for hyper-parameter optimization. J. Mach. Learn. Res. 13, 281–305. https://doi.org/10.1162/153244303322533223.

Bhagat, Y. a, Hussain, M.S., Stobbe, R.W., Butcher, K.S., Emery, D.J., Shuaib, A., Siddiqui, M.M., Maheshwari, P., Al-Hussain, F., Beaulieu, C., 2008. Elevations of diffusion anisotropy are associated with hyper-acute stroke: a serial imaging study. Magn. Reson. Imaging 26, 683–693. https://doi.org/10.1016/j.mri.2008.01.015.

Budde, M.D., Frank, J.A., 2010. Neurite beading is sufficient to decrease the apparent diffusion coefficient after ischemic stroke. Proc. Natl. Acad. Sci. 107, 14,472–14,477. https://doi.org/10.1073/pnas.1004841107.

Chawla, N.V., Bowyer, K.W., Hall, L.O., Kegelmeyer, W.P., 2002. SMOTE: Synthetic minority over-sampling technique. J. Artif. Intell. Res. 16, 321–357. https://doi.org/10.1613/jair.953.

Cheng, B., Forkert, N.D., Zavaglia, M., Hilgetag, C.C., Golsari, A., Siemonsen, S., Fiehler, J., Pedraza, S., Puig, J., Cho, T.H., Alawneh, J., Baron, J.C., Ostergaard, L., Gerloff, C., Thomalla, G., 2014. Influence of stroke infarct location on functional outcome measured by the modified rankin scale. Stroke 45, 1695–1702. https://doi.org/10.1161/STROKEAHA.114.005152.

Corbetta, M., Ramsey, L., Callejas, A., Baldassarre, A., Hacker, C.D., Siegel, J.S., Astafiev, S.V., Rengachary, J., Zinn, K., Lang, C.E., Connor, L.T., Fucetola, R., Strube, M., Carter, A.R., Shulman, G.L., 2015. Common behavioral clusters and subcortical anatomy in stroke. Neuron 85, 927–941. https://doi.org/10.1016/j.neuron.2015.02.027.

Cuingnet, R., Rosso, C., Chupin, M., Lehéricy, S., Dormont, D., Benali, H., Samson, Y., Colliot, O., 2011. Spatial regularization of SVM for the detection of diffusion alterations associated with stroke outcome. Med. Image Anal. 15, 729–737. https://doi.org/10.1016/j.media.2011.05.007.

Doughty, C., Wang, J., Feng, W., Hackney, D., Pani, E., Schlaug, G., 2016. Detection and predictive value of fractional anisotropy changes of the corticospinal tract in the acute phase of a stroke. Stroke 47, 1520–1526. https://doi.org/10.1161/STROKEAHA.115.012088.

Duncan, P.W., Jorgensen, H.S., Wade, D.T., 2000. Outcome measures in acute stroke trials: a systematic review and some recommendations to improve practice. Stroke 31, 1429–1438.

Ernst, M., Boers, A.M.M., Forkert, N.D., Berkhemer, O.A., Roos, Y.B., Dippel, D.W.J., van der Lugt, A., van Oostenbrugge, R.J., van Zwam, W.H., Vettorazzi, E., Fiehler, J., Marquering, H.A., Majoie, C.B.L.M., Gellissen, S., MR CLEAN trial investigators (www.mrclean-trial.org), 2018. Impact of ischemic lesion location on the mRS score in patients with ischemic stroke: a voxel-based approach. AJNR Am. J. Neuroradiol. 1–6. https://doi.org/10.3174/ajnr.A5821.

Groisser, B.N., Copen, W.A., Singhal, A.B., Hirai, K.K., Schaechter, J.D., 2014. Corticospinal tract diffusion abnormalities early after stroke predict motor outcome. Neurorehabil. Neural Repair 28, 751–760. https://doi.org/10.1177/1545968314521896.

Jauch, E.C., Saver, J.L., Adams, H.P., Bruno, A., Connors, J.J., Demaerschalk, B.M., Khatri, P., McMullan, P.W., Qureshi, A.I., Rosenfield, K., Scott, P.A., Summers, D.R., Wang, D.Z., Wintermark, M., Yonas, H., 2013. Guidelines for the early management of patients with acute ischemic stroke: a guideline for healthcare professionals from the American heart association/American stroke association. Stroke 44, 870–947. https://doi.org/10.1161/STR.0b013e318284056a.

Lemm, S., Blankertz, B., Dickhaus, T., Müller, K.R., 2011. Introduction to machine learning for brain imaging. Neuroimage 56, 387–399. https://doi.org/10.1016/j.neuroimage.2010.11.004.

Liang, D., Bhatta, S., Gerzanich, V., Simard, J.M., 2007. Cytotoxic edema: mechanisms of pathological cell swelling. Neurosurg. Focus. 22, E2.

Liu, G., Peng, K., Dang, C., Tan, S., Chen, H., Xie, C., Xing, S., Zeng, J., 2018. Axial diffusivity changes in the motor pathway above stroke foci and functional recovery after subcortical infarction. Restor. Neurol. Neurosci. 36, 173–182. https://doi.org/10.3233/RNN-170747.

Mah, Y.H., Husain, M., Rees, G., Nachev, P., 2014. Human brain lesion-deficit inference remapped. Brain 137, 2522–2531. https://doi.org/10.1093/brain/awu164.

Marchina, S., Zhu, L.L., Norton, A., Zipse, L., Wan, C.Y., Schlaug, G., 2011. Impairment of speech production predicted by lesion load of the left arcuate fasciculus. Stroke 42, 2251–2256. https://doi.org/10.1161/STROKEAHA.110.606103.

Mateos-Pérez, J.M., Dadar, M., Lacalle-Aurioles, M., Iturria-Medina, Y., Zeighami, Y., Evans, A.C., 2018. Structural neuroimaging as clinical predictor: a review of machine learning applications. Neuro Image Clin. 20, 506–522. https://doi.org/10.1016/j.nicl.2018.08.019.

Moulton, E., Amor-Sahli, M., Perlbarg, V., Pires, C., Crozier, S., Galanaud, D., Valabregue, R., Yger, M., Baronnet-Chauvet, F., Samson, Y., Dormont, D., Rosso, C., 2015. Axial diffusivity of the corona radiata at 24 h post-stroke: a new biomarker for motor and global outcome. PLoS One 10, 1–16. https://doi.org/10.1371/journal.pone.0142910.

Moulton, E., Valabrègue, R., Díaz, B., Kemlin, C., Leder, S., Lehéricy, S., Samson, Y., Rosso, C., Valabregue, R., Díaz, B., Kemlin, C., Leder, S., Lehéricy, S., Samson, Y., Rosso, C., 2018. Comparison of spatial normalization strategies of diffusion MRI data for studying motor outcome in subacute-chronic and acute stroke. Neuroimage 183, 186–199. https://doi.org/10.1016/j.neuroimage.2018.08.002.

Muñoz Maniega, S., Bastin, M.E., Armitage, P. a, Farrall, A.J., Carpenter, T.K., Hand, P.J., Cvoro, V., Rivers, C.S., Wardlaw, J.M., 2004. Temporal evolution of water diffusion parameters is different in grey and white matter in human ischaemic stroke. J. Neurol. Neurosurg. Psychiatry 75, 1714–1718. https://doi.org/10.1136/jnnp.2003.033852.

Munsch, F., Sagnier, S., Asselineau, J., Bigourdan, A., Guttmann, C.R., Debruxelles, S., Poli, M., Renou, P., Perez, P., Dousset, V., Sibon, I., Tourdias, T., 2016. Stroke location is an independent predictor of cognitive outcome. Stroke 47, 66–73. https://doi.org/10.1161/STROKEAHA.115.011242.

Nadeau, C., Bengio, Y., 2003. Inference for the generalization error. Mach. Learn. 52, 239–281. https://doi.org/10.1023/A:1024068626366.

Phan, T.G., Donnan, G.A., Wright, P.M., Reutens, D.C., 2005. A digital map of middle cerebral artery infarcts associated with middle cerebral artery trunk and branch occlusion. Stroke 36, 986–991. https://doi.org/10.1161/01.STR.0000163087.66828.e9.

Phan, T.G., Chen, J., Donnan, G., Srikanth, V., Wood, A., Reutens, D.C., 2010. Development of a new tool to correlate stroke outcome with infarct topography: A proof-of-concept study. Neuroimage 49, 127–133. https://doi.org/10.1016/j.neuroimage.2009.07.067.

Price, C.J., Hope, T.M., Seghier, M.L., 2017. Ten problems and solutions when predicting individual outcome from lesion site after stroke. Neuroimage 145, 200–208. https://doi.org/10.1016/j.neuroimage.2016.08.006.

Rehme, A.K., Volz, L.J., Feis, D.L., Bomilcar-Focke, I., Liebig, T., Eickhoff, S.B., Fink, G.R., Grefkes, C., 2015a. Identifying neuroimaging markers of motor disability in acute stroke by machine learning techniques. Cereb. Cortex 25, 3046–3056. https://doi.org/10.1093/cercor/bhu100.

Rehme, A.K., Volz, L.J., Feis, D.L., Eickhoff, S.B., Fink, G.R., Grefkes, C., 2015b. Individual prediction of chronic motor outcome in the acute post-stroke stage: Behavioral parameters versus functional imaging. Hum. Brain Mapp. 36, 4553–4565. https://doi.org/10.1002/hbm.22936.

Rondina, J.M., Filippone, M., Girolami, M., Ward, N.S., 2016. Decoding post-stroke motor function from structural brain imaging. Neuro Image Clin. 12, 372–380. https://doi.org/10.1016/j.nicl.2016.07.014.

Rondina, J.M., Park, C.H., Ward, N.S., 2017. Brain regions important for recovery after severe post-stroke upper limb paresis. J. Neurol. Neurosurg. Psychiatry 88, 737–743. https://doi.org/10.1136/jnnp-2016-315030.

Rosso, C., Colliot, O., Valabrègue, R., Crozier, S., Dormont, D., Lehéricy, S., Samson, Y., 2011. Tissue at risk in the deep middle cerebral artery territory is critical to stroke outcome. Neuroradiology 53, 763–771. https://doi.org/10.1007/s00234-011-0916-5.

Rosso, C., Vargas, P., Valabregue, R., Arbizu, C., Henry-Amar, F., Leger, A., Lehéricy, S., Samson, Y., 2015. Aphasia severity in chronic stroke patients: a combined disconnection in the dorsal and ventral language pathways. Neurorehabil. Neural Repair 29, 287–295. https://doi.org/10.1177/1545968314543926.

Samper-González, J., Burgos, N., Bottani, S., Fontanella, S., Lu, P., Marcoux, A., Routier, A., Guillon, J., Bacci, M., Wen, J., Bertrand, A., Bertin, H., Habert, M.-O., Durrleman, S., Evgeniou, T., Colliot, O., 2018. Reproducible evaluation of classification methods in Alzheimer's disease: Framework and application to MRI and PET data. Neuroimage 183, 504–521. https://doi.org/10.1016/j.neuroimage.2018.08.042.

Saur, D., Ronneberger, O., Kümmerer, D., Mader, I., Weiller, C., Klöppel, S., 2010. Early functional magnetic resonance imaging activations predict language outcome after stroke. Brain 133, 1252–1264. https://doi.org/10.1093/brain/awq021.

Siegel, J.S., Ramsey, L.E., Snyder, A.Z., Metcalf, N.V., Chacko, R.V., Weinberger, K., Baldassarre, A., Hacker, C.D., Shulman, G.L., Corbetta, M., 2016. Disruptions of network connectivity predict impairment in multiple behavioral domains after stroke. Proc. Natl. Acad. Sci. U. S. A. 113, E4367–E4376. https://doi.org/10.1073/pnas.1521083113.

Smith, S.M., 2002. Fast robust automated brain extraction. Hum. Brain Mapp. 17, 143–155. https://doi.org/10.1002/hbm.10062.

Smith, S.M., Jenkinson, M., Woolrich, M.W., Beckmann, C.F., Behrens, T.E.J., Johansen-Berg, H., Bannister, P.R., De Luca, M., Drobnjak, I., Flitney, D.E., Niazy, R.K., Saunders, J., Vickers, J., Zhang, Y., De Stefano, N., Brady, J.M., Matthews, P.M., 2004. Advances in functional and structural MR image analysis and implementation as FSL. Neuroimage 23 (Suppl. 1), S208–S219. https://doi.org/10.1016/j.neuroimage.2004.07.051.

Sotak, C.H., 2002. The role of diffusion tensor imaging in the evaluation of ischemic brain injury - a review. NMR Biomed. 15, 561–569. https://doi.org/10.1002/nbm.786.

Spampinato, M.V., Chan, C., Jensen, J.H., Helpern, J.A., Bonilha, L., Kautz, S.A., Nietert, P.J., Feng, W., 2017. Diffusional kurtosis imaging and motor outcome in acute ischemic stroke. Am. J. Neuroradiol. 1–7. https://doi.org/10.3174/ajnr.A5180.

Sun, S.-W., Liang, H.-F., Le, T.Q., Armstrong, R.C., Cross, A.H., Song, S.-K., 2006. Differential sensitivity of in vivo and ex vivo diffusion tensor imaging to evolving optic nerve injury in mice with retinal ischemia. Neuroimage 32, 1195–1204. https://doi.org/10.1016/j.neuroimage.2006.04.212.

Thiebaut de Schotten, M., Tomaiuolo, F., Aiello, M., Merola, S., Silvetti, M., Lecce, F., Bartolomeo, P., Doricchi, F., 2014. Damage to white matter pathways in subacute and chronic spatial neglect: a group study and 2 single-case studies with complete virtual "in vivo" tractography dissection. Cereb. Cortex 24, 691–706. https://doi.org/10.1093/cercor/bhs351.

Toga, A.W., Thompson, P.M., 2003. Mapping brain asymmetry. Nat. Rev. Neurosci. 4, 37–48. https://doi.org/10.1038/nrn1009.

Varoquaux, G., 2018. Cross-validation failure: Small sample sizes lead to large error bars. Neuroimage 180, 68–77. https://doi.org/10.1016/j.neuroimage.2017.06.061.

Varoquaux, G., Raamana, P.R., Engemann, D.A., Hoyos-Idrobo, A., Schwartz, Y., Thirion, B., 2017. Assessing and tuning brain decoders: Cross-validation, caveats, and guidelines. Neuroimage 145, 166–179. https://doi.org/10.1016/j.neuroimage.2016.10.038.

Veraart, J., Fieremans, E., Novikov, D.S., 2016a. Diffusion MRI noise mapping using random matrix theory. Magn. Reson. Med. 76, 1582–1593. https://doi.org/10.1002/mrm.26059.

Veraart, J., Novikov, D.S., Christiaens, D., Ades-aron, B., Sijbers, J., Fieremans, E., 2016b.

Denoising of diffusion MRI using random matrix theory. Neuroimage 142, 394–406. https://doi.org/10.1016/j.neuroimage.2016.08.016.

Wu, O., Cloonan, L., Mocking, S.J.T., Bouts, M.J.R.J., Copen, W.A., Cougo-Pinto, P.T., Fitzpatrick, K., Kanakis, A., Schaefer, P.W., Rosand, J., Furie, K.L., Rost, N.S., 2015. Role of acute lesion topography in initial ischemic stroke severity and long-term functional outcomes. Stroke 46, 2438–2444. https://doi.org/10.1161/STROKEAHA.115.009643.

Yang, Q., Tress, B.M., Barber, P.A., Desmond, P.M., Darby, D.G., Gerraty, R.P., Li, T., Davis, S.M., Barber, Alan, P., Desmond, P.M., Darby, D.G., Gerraty, R.P., Li, T., Davis, S.M., 1999. Serial study of apparent diffusion coefficient and anisotropy in patients with acute stroke. Stroke 30, 2382–2390. https://doi.org/10.1161/01.STR.30.11.2382.

Yoo, A.J., Barak, E.R., Copen, W. a, Kamalian, S., Gharai, L.R., Pervez, M. a, Schwamm, L.H., González, R.G., Schaefer, P.W., 2010. Combining acute diffusion-weighted imaging and mean transmit time lesion volumes with National Institutes of Health Stroke Scale Score improves the prediction of acute stroke outcome. Stroke. 41, 1728–1735. https://doi.org/10.1161/STROKEAHA.110.582874.

Yourganov, G., Smith, K.G., Fridriksson, J., Rorden, C., 2015. Predicting aphasia type from brain damage measured with structural MRI. Cortex 73, 203–215. https://doi.org/10.1016/j.cortex.2015.09.005.

Zhang, Y., Brady, M., Smith, S., 2001. Segmentation of brain MR images through a hidden Markov random field model and the expectation-maximization algorithm. IEEE Trans. Med. Imaging 20, 45–57. https://doi.org/10.1109/42.906424.

Zhang, Y., Kimberg, D.Y., Coslett, H.B., Schwartz, M.F., Wang, Z., 2014. Multivariate lesion-symptom mapping using support vector regression. Hum. Brain Mapp. 35, 5861–5876. https://doi.org/10.1002/hbm.22590.